Human dental pulp-derived stem cells promote locomotor recovery after complete transection of the rat spinal cord by multiple neuro-regenerative mechanisms

Kiyoshi Sakai,[1] Akihito Yamamoto,[1] Kohki Matsubara,[1] Shoko Nakamura,[1] Mami Naruse,[1] Mari Yamagata,[1] Kazuma Sakamoto,[2] Ryoji Tauchi,[3] Norimitsu Wakao,[3] Shiro Imagama,[3] Hideharu Hibi,[1] Kenji Kadomatsu,[2] Naoki Ishiguro,[3] and Minoru Ueda[1]

[1]Department of Oral and Maxillofacial Surgery, [2]Department of Biochemistry, and
[3]Department of Orthopedic Surgery, Nagoya University Graduate School of Medicine, Nagoya, Japan.

Spinal cord injury (SCI) often leads to persistent functional deficits due to loss of neurons and glia and to limited axonal regeneration after injury. Here we report that transplantation of human dental pulp stem cells into the completely transected adult rat spinal cord resulted in marked recovery of hind limb locomotor functions. Transplantation of human bone marrow stromal cells or skin-derived fibroblasts led to substantially less recovery of locomotor function. The human dental pulp stem cells exhibited three major neuroregenerative activities. First, they inhibited the SCI-induced apoptosis of neurons, astrocytes, and oligodendrocytes, which improved the preservation of neuronal filaments and myelin sheaths. Second, they promoted the regeneration of transected axons by directly inhibiting multiple axon growth inhibitors, including chondroitin sulfate proteoglycan and myelin-associated glycoprotein, via paracrine mechanisms. Last, they replaced lost cells by differentiating into mature oligodendrocytes under the extreme conditions of SCI. Our data demonstrate that tooth-derived stem cells may provide therapeutic benefits for treating SCI through both cell-autonomous and paracrine neuroregenerative activities.

Introduction

The development of effective treatments for spinal cord injury (SCI) has been stifled by this injury's complicated pathophysiology (1). During the acute phase, the focal mechanical insult disrupts tissue homeostasis. This triggers secondary injury processes in which multiple destructive cascades cause the necrotic and apoptotic death of neurons, astrocytes, and oligodendrocytes, which spreads beyond the initial injury site and leads to irreversible axonal damage and demyelination (2, 3). Subsequently, reactive astrocytes and oligodendrocytes near the site of injured spinal cord (SC) respectively produce chondroitin sulfate proteoglycans (CSPGs) and myelin proteins (including myelin-associated glycoprotein [MAG], Nogo, oligodendrocyte myelin glycoprotein [OMgp], netrin, semaphorin, and ephrin). These extracellular molecules function as axon growth inhibitors (AGIs), acting through the intracellular Rho GTPase signaling cascade (4). These multiple pathogenic signals synergistically accelerate the progressive deterioration after SCI. Therefore, therapeutic strategies for functional recovery from SCI must exert multifaceted reparative effects against a variety of pathogeneses (2).

Stem cell–based transplantation therapy holds great promise for establishing such a multifaceted therapeutic strategy. In the last decade, a variety of cell types, including human neural stem cells (5), embryonic stem cell derivatives (6–8), and adult bone marrow stromal cells (BMSCs) (9, 10), have been transplanted into the injured SC of rats or mice, and their neuroregenerative activities evaluated. These preclinical studies showed that engrafted stem cells promote substantial functional recovery after SCI through both cell-autonomous/cell-replacement and paracrine/trophic effects (11). However, the previously tested stem cells show poor survival (6–8, 12) and/or differentiation under the severe conditions of SCI (9, 13, 14), and the transplantation of individual stem cells has led to only modest therapeutic benefits. Furthermore, although the trophic factors derived from these stem cells promote in vitro neurite extension and survival, their roles in the functional recovery of SCI are still largely unknown.

Human adult dental pulp stem cells (DPSCs) and stem cells from human exfoliated deciduous teeth (SHEDs) are self-renewing stem cells residing within the perivascular niche of the dental pulp (15). They are thought to originate from the cranial neural crest and express early markers for both mesenchymal and neuroectodermal stem cells (16, 17). Since naturally exfoliated deciduous and impacted adult wisdom teeth are not usually needed, DPSCs and SHEDs can be obtained without adverse health effects. Similar to BMSCs, these cells are able to differentiate into osteoblasts, chondrocytes, adipocytes, endothelial cells, and functionally active neurons in vitro, under defined conditions (16–19). Trophic factors expressed by them promote neuronal survival, proliferation, differentiation, and migration (20–23). Thus, these previous reports support the use of tooth-derived stem cells as a unique cellular resource for neuroregeneration therapies. However, their ability to promote functional recovery in neurological disorders remains largely unknown.

Table 1
Flow cytometry of stem cells from humans

	SHEDs (*n* = 3)		DPSCs (*n* = 3)		BMSCs (*n* = 3)	
	Positive (%)	SD	Positive (%)	SD	Positive (%)	SD
MSC markers						
CD90	98.25	0.91	98.96	0.95	≥90	
CD73	91.45	8.44	96.60	2.14	≥90	
CD105	98.20	2.44	98.23	0.54	≥90	
Negative markers						
CD45	0.33	0.28	0.11	0.09	≤10	
CD34	0.36	0.32	0.07	0.03	≤10	
CD11b	0.02	0.02	0.03	0.02	≤10	
HLA-DR	0.45	0.39	0.12	0.10	≤10	
Neural markers						
DCX	95.42	0.66	84.45	0.45	91.37	8.20
Nestin	92.71	10.46	95.40	1.52	35.76	8.06
GFAP	92.93	8.30	97.50	3.54	4.49	3.11
βIII-Tubulin	99.69	0.21	85.43	0.77	99.24	0.73
NeuN	31.93	7.25	26.61	4.28	2.97	1.74
A2B5	94.84	3.72	96.34	0.33	35.47	15.07
CNPase	99.21	0.11	98.19	0.46	21.35	7.81
APC	0.20	0.01	0.36	0.02	2.75	2.05
MBP	0.68	0.04	0.32	0.02	3.02	2.00

Here we examined the neuroregenerative activities of DPSCs and SHEDs by transplanting them into a completely transected rat SCI model during the acute phase, in which axonal regeneration rather than axonal sprouting can be evaluated accurately. Our data show that these tooth-derived stem cells promoted functional recovery after SCI by multifaceted neuro-regenerative activities, via both cell-autonomous/cell replacement and paracrine/trophic mechanisms.

Results

Characterization of isolated human SHEDs and DPSCs for use in transplantation studies. Flow cytometry analysis showed that the SHEDs and DPSCs expressed a set of mesenchymal stem cell (MSC) markers (i.e., CD90, CD73, and CD105), but not endothelial/hematopoietic markers (i.e., CD34, CD45, CD11b/c, and HLA-DR) (Table 1). Like human BMSCs, both the SHEDs and DPSCs exhibited adipogenic, chondrogenic, and osteogenic differentiation as described previously (refs. 16, 17, and data not shown). The majority of SHEDs and DPSCs coexpressed several neural lineage markers: nestin (neural stem cells), doublecortin (DCX; neuronal progenitor cells), βIII-tubulin (early neuronal cells), NeuN (mature neurons), GFAP (neural stem cells and astrocytes), S-100 (Schwann cells), and A2B5 and CNPase (oligodendrocyte progenitor cells), but not adenomatous polyposis coli (APC) or myelin basic protein (MBP) (mature oligodendrocytes) (Figure 1A and Table 1). This expression profile was confirmed by immunohistochemical analyses (Figure 1B).

Next, we examined the expression of representative neurotrophic factors by real-time PCR. Both the SHEDs and DPSCs expressed glial cell–derived neurotrophic factor (*GDNF*), brain-derived neurotrophic factor (*BDNF*), and ciliary neurotrophic factor (*CNTF*) at more than 3 to 5 times the levels expressed by skin-derived fibroblasts or BMSCs (Figure 1C).

We further characterized the transcriptomes of SHEDs and BMSCs by cDNA microarray analysis. This gene expression analysis revealed a 2.0-fold difference in the expression of 3,318 of 41,078 genes between SHEDs and BMSCs. Of these, 1,718 genes were expressed at higher levels in the SHEDs and 1,593 genes were expressed at lower levels (data not shown). The top 30 genes showing higher expression in the SHEDs were in the following ontology categories: extracellular and cell surface region, cell proliferation, and tissue/embryonic development (Table 2).

SHEDs and DPSCs promoted locomotor recovery after SCI. To compare the neuroregenerative activities of human SHEDs and DPSCs with those of human BMSCs and human skin fibroblasts, we transplanted the cells into the completely transected SCs, as described in Methods, and evaluated locomotion recovery using the Basso, Beattie, Bresnahan locomotor rating scale (BBB scale) (24). Remarkably, the animals that received SHEDs or DPSCs exhibited a significantly higher BBB score during the entire observation period, compared with BMSC-transplanted, fibroblast-transplanted, or PBS-injected control rats (Figure 2A). Importantly, their superior recoveries were evident soon after the operation, during the acute phase of SCI. After the recovery period (5 weeks after the operation), the rats that had received SHEDs were able to move 3 joints of hind limb coordinately and walk without weight support (*P* < 0.01; Supplemental Videos 1 and 2), while the BMSC- or fibroblast-transplanted rats exhibited only subtle movements of 1–2 joints. These results demonstrate that the transplantation of SHEDs or DPSCs during the acute phase of SCI significantly improved the recovery of hind limb locomotor function. Since the level of recovery was similar in the SHED- and DPSC-transplanted rats, we focused on the phenotypical examination of SHED-transplanted rats to elucidate how tooth-derived stem cells promoted the regeneration of the completely transected rat SC.

SHEDs regenerated the transected corticospinal tract and raphespinal serotonergic axons. To examine whether engrafted SHEDs affect the preservation of neurofilaments, we performed immunohistochemical analyses with an anti–neurofilament M (NF-M) mAb, 8 weeks after transection. Compared with the PBS-treated control SCs, the SHED-transplanted SCs exhibited greater preservation of NF-positive axons from 3 mm rostral to 3 mm caudal to the transected lesion site (Figure 2, B and C; asterisk indicates epicenter). The percentages of NF-positive axons in the epicenter of the SHED-transplanted and control SCs were 35.8% ± 13.0% and 8.7% ± 3.4%, respectively, relative to sham-treated SCs (Figure 2D).

Regeneration of both the corticospinal tract (CST) and the descending serotonergic raphespinal axons is important for the recovery of hind limb locomotor function in rat SCI. We therefore examined whether these axons had extended beyond the epicenter in the SHED-transplanted SCs. The CST axons were traced with the anterograde tracer biotinylated dextran amine (BDA), which was injected into the sensorimotor cortex. The serotoner-
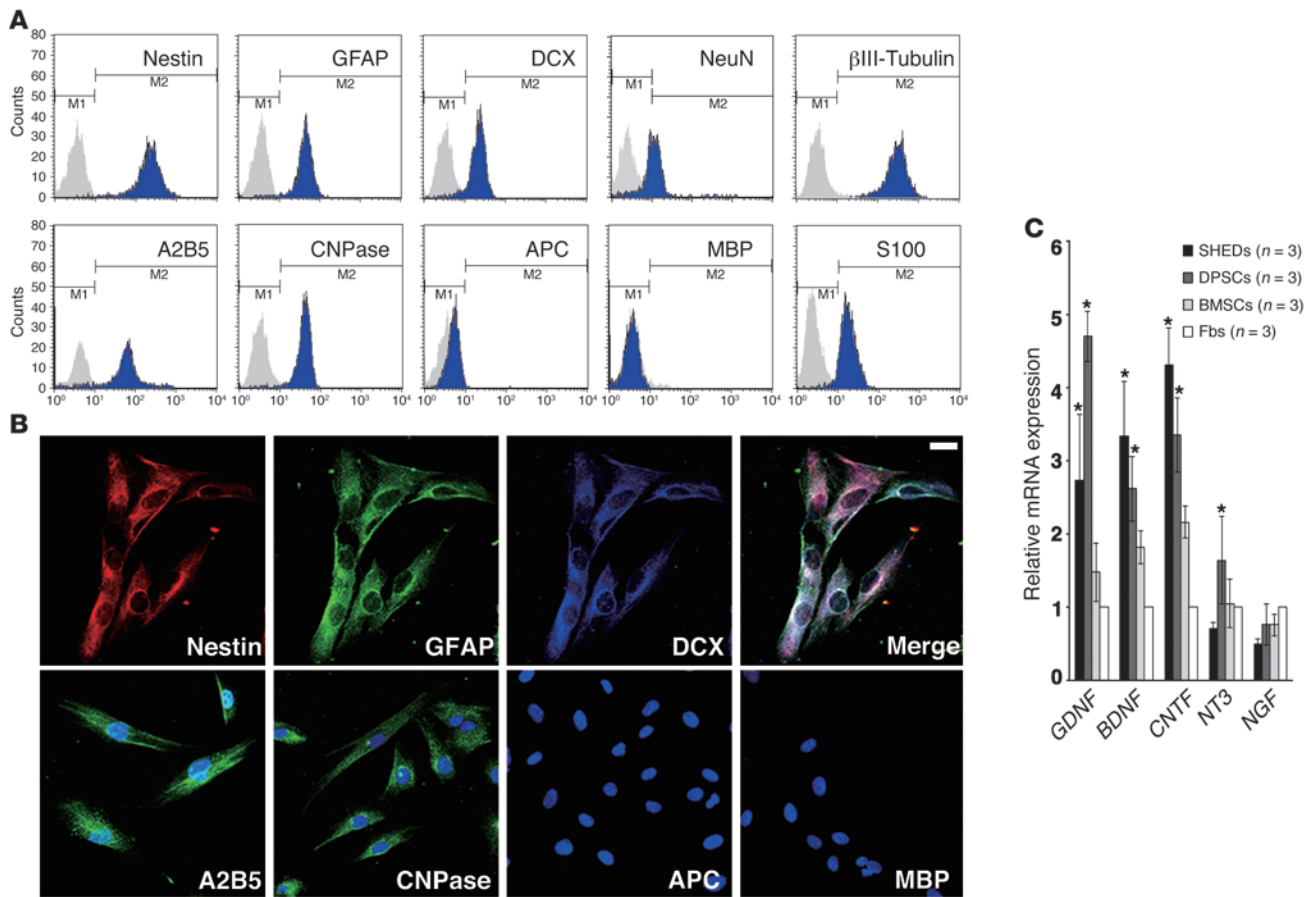
Figure 1
Characterization of the SHEDs and DPSCs used for transplantation. (**A**) Flow cytometry analysis of the neural cell lineage markers expressed in SHEDs. Note that most of the SHEDs and DPSCs coexpressed neural stem and multiple progenitor markers, but not mature oligodendrocytes (APC and MBP). (**B**) Confocal images showing SHEDs coexpressed nestin, GFAP, and DCX. SHEDs also expressed markers for oligodendrocyte progenitor cells (A2B5 and CNPase), but not for mature oligodendrocytes (APC and MBP). Scale bar: 10 μm. (**C**) Real-time RT-PCR analysis of the expression of neurotrophic factors. Results are expressed as fold increase compared with the level expressed in skin fibroblasts. Data represent the average measurements for each cell type from 3 independent donors. This set of experiments was repeated twice and yielded similar results. Data represent the mean ± SEM. *$P < 0.01$ compared with BMSCs and fibroblasts (Fbs).

gic raphespinal axons were immunohistochemically detected by a mAb that specifically reacts with serotonin (5-hydroxytryptamine [5-HT]), which is synthesized within the brain stem. We found that both BDA- and 5-HT–positive fibers extended as far as 3 mm caudal to the epicenter in the SHED-transplanted but not the control group (Figures 3 and 4). Furthermore, some BDA- and 5-HT–positive boutons could be seen apposed to neurons in the caudal stump (Figure 3D and Figure 4C), suggesting that the regenerated axons had established new neural connections. Notably, although the number of descending axons extending beyond the epicenter was small, we observed many of them penetrating the scar tissue of the rostral stump (Figure 3A and Figure 4A). The percentages of 5-HT–positive axons of the SHED-transplanted SCs at 1 and 3 mm rostral to the epicenter were 58.9% ± 3.9% and 78.3% ± 7.4% relative to sham-treated SC, respectively (Figure 4D). These results demonstrate that the engrafted SHEDs promoted the recovery of hind limb locomotion via the preservation and regeneration of transected axons, even in the microenvironment of the damaged CNS.

SHEDs inhibited the Rho GTPase activity induced by SC transection. The apparent axon regeneration in the SHED-transplanted SCs suggested that the SHEDs might modulate multiple AGI signals generated from oligodendrocytes and reactive astrocytes forming the glial scar. We therefore measured the activity level of Rho GTPase, which is an intracellular target of multiple AGIs, by pull-down assay. The injured SCs were isolated 7 days after transection and subjected to immunoprecipitation with GST-tagged Rho-binding domain (RBD). The level of active Rho (GTP-bound Rho [GTP-Rho]) in the transected control SCs increased; however, the engrafted SHEDs remarkably inhibited the activation of Rho (Figure 4E). These results strongly suggest that SHEDs promoted axon regeneration through the inhibition of multiple AGI signals.

Serum-free conditioned medium from both SHEDs and DPSCs antagonizes CSPG- or MAG-mediated neurite growth inhibition. Next, to analyze the roles of trophic mechanisms in the SHED-mediated axon regeneration, we examined whether the conditioned medium (CM) from SHEDs (SHED-CM) or DPSCs (DPSC-CM) could promote the neurite extension of cerebral granular neurons (CGNs)

Table 2

Functional gene classification in SHEDs versus BMSCs

Term	Changed gene up	Total gene	P
Extracellular region	343	2,865	2.52×10^{-14}
Skeletal system development	104	661	1.46×10^{-9}
Extracellular matrix	101	678	9.20×10^{-9}
Extracellular space	147	1,134	2.00×10^{-8}
Extracellular matrix organization	43	195	4.86×10^{-8}
Multicellular organismal development	643	6,683	9.36×10^{-8}
Collagen fibril organization	20	57	4.97×10^{-7}
Anatomical structure morphogenesis	346	3,339	9.52×10^{-7}
Mitotic cell cycle	146	1,184	1.11×10^{-6}
Proteinaceous extracellular matrix	82	578	1.36×10^{-6}
Organ morphogenesis	144	1,182	2.43×10^{-6}
Vasculature development	98	732	3.76×10^{-6}
Embryonic morphogenesis	96	728	7.04×10^{-6}
Cell proliferation	245	2,288	7.17×10^{-6}
Cell cycle	230	2,135	9.74×10^{-6}
Blood vessel development	93	707	1.31×10^{-5}
Response to wounding	191	1,738	2.02×10^{-5}
Receptor protein serine/ threonine kinase signaling	56	369	2.12×10^{-5}
M phase of mitotic cell cycle	77	567	2.40×10^{-5}
Cell surface	86	671	3.26×10^{-5}
Organ development	362	3,675	3.68×10^{-5}
Collagen binding	21	90	3.90×10^{-5}
Glycosaminoglycan binding	42	262	4.65×10^{-5}
Mitotic spindle organization	12	33	7.15×10^{-5}
Cell adhesion	183	1,693	7.76×10^{-5}
Skeletal system morphogenesis	42	260	8.16×10^{-5}
Tissue development	185	1,720	8.76×10^{-5}
Cell surface receptor linked signaling pathway	368	3,785	8.98×10^{-5}
Mitosis	73	554	9.98×10^{-5}
Regulation of cell cycle	127	1,103	0.000109

on dishes coated with an AGI. CGNs isolated from newborn rats extended neurites on poly-L-lysine (PLL), but not on CSPG or MAG. Remarkably, both SHED-CM and DPSC-CM restored neurite extension activity of CGNs, while CM from fibroblasts (fibroblast-CM) or BMSCs (BMSC-CM) exhibited only subtle extension (Figure 5). Quantitative analysis showed that neurite extension through the inhibition of multiple AGIs was a unique characteristic of the tooth-derived stem cell (Figure 5, L and M). These results demonstrate that both SHEDs and DPSCs promote the regeneration of transected axons though direct inhibition of the multiple AGI signals by paracrine mechanisms.

SHEDs inhibited myelin degeneration. Next, we examined whether transplanted SHEDs preserved myelination in the transected SC by immunohistochemical staining with the fluorescent dye FluoroMyelin. In transverse sections of sham-operated SCs, white matter was clearly labeled by FluoroMyelin, and gray matter was not (data not shown). The control SCs exhibited little or no staining at the epicenter or 3 mm caudal to it (Figure 6, C and D). In contrast, we found significant FluoroMyelin-positive spots in the epicenter of the SHED-transplanted SCs, indicating that the SHEDs caused the regeneration of myelin structures in the transected region (Figure 6A). Notably, the myelin-positive areas of the SHED-transplanted SCs at 3 and 4 mm caudal to the epicenter constituted 55.3% ± 4.5% and 78.0% ± 4.1%, respectively, of the

same areas in the sham-operated SCs, demonstrating that the SHEDs exerted remarkable myelin preservation activity (Figure 6E).

SHEDs survived and specifically differentiated into oligodendrocytes in the injured SC. In the FluoroMyelin-stained sections, we observed a myelin-expressing cell cluster in the gray matter of SHED-transplanted SCs (Figure 6B). We anticipated that these myelin-expressing cells would be mature oligodendrocytes derived from the transplanted SHEDs. To assess this possibility, we performed immunohistological analyses using anti–human nuclear antigen (HuNu) and two mature oligodendrocyte markers, APC and MBP (25, 26). Eight weeks after grafting, 32.3% ± 3.1% of the transplanted SHEDs still survived in the injured SCs (data not shown). Of these cells, 86.2% ± 6.2% and 90.2% ± 4.6% expressed APC and MBP, respectively (Figure 7). In addition, 10% of the HuNu-positive cells were negative for MBP and APC, but their fate is currently unknown (data not shown). Before the transplantation, SHEDs expressed many early neural cell lineage markers (Figure 1 and Table 1). However, the surviving transplanted SHEDs did not express NF-M or GFAP (Figure 7), indicating that they specifically differentiated along the oligodendrocyte lineage in the injured SCs.

SHEDs inhibited neuronal and glial apoptosis after SCI. SCI-induced cell death is a major contributor to secondary injury, in which irreversible tissue damage spreads across the SC. Twenty-four hours after injury, at 1 mm caudal to the epicenter, most of the cells expressing NeuN, GFAP, or MBP were costained with TUNEL, showing that massive multicellular apoptosis occurred immediately after SCI (Figure 8). The engrafted SHEDs significantly decreased the TUNEL staining in all 3 of these lineages (Figure 8, C, D, G, H, K, and L): The total number of TUNEL-positive cells in the SHED-transplanted SCs was approximately 20% of that in the control SCs (Figure 8M). The percentages of TUNEL-positive cells in the control and SHED-transplanted SCs were 87.7% ± 3.1% and 3.1% ± 3.2%, respectively (Figure 8N). These results demonstrate that the transplanted SHEDs minimized the expansion of secondary injury through strong neuroprotection of all the neural cell lineages.

Discussion

We report here the remarkable neuroregenerative activity of tooth-derived stem cells, SHEDs and DPSCs, for functional recovery after SCI. Previous studies have dealt with the differentiation characteristics of tooth-derived stem cells (16–19) and their trophic effects on the proliferation, migration, and survival of particular subsets of neurons (20–23). However, few studies have considered the therapeutic benefits of these stem cells for a particular neurological disorder. Our study revealed that engrafted SHEDs exhibited three major therapeutic benefits for recovery after SCI, including (a) inhibition of SCI-induced apoptosis of neurons, astrocytes, and oligodendrocytes, which promoted the preservation of neural fibers and myelin sheaths; (b) regeneration of the transected axon through the direct inhibition of multiple AGI signals, such as CSPGs and MAG,
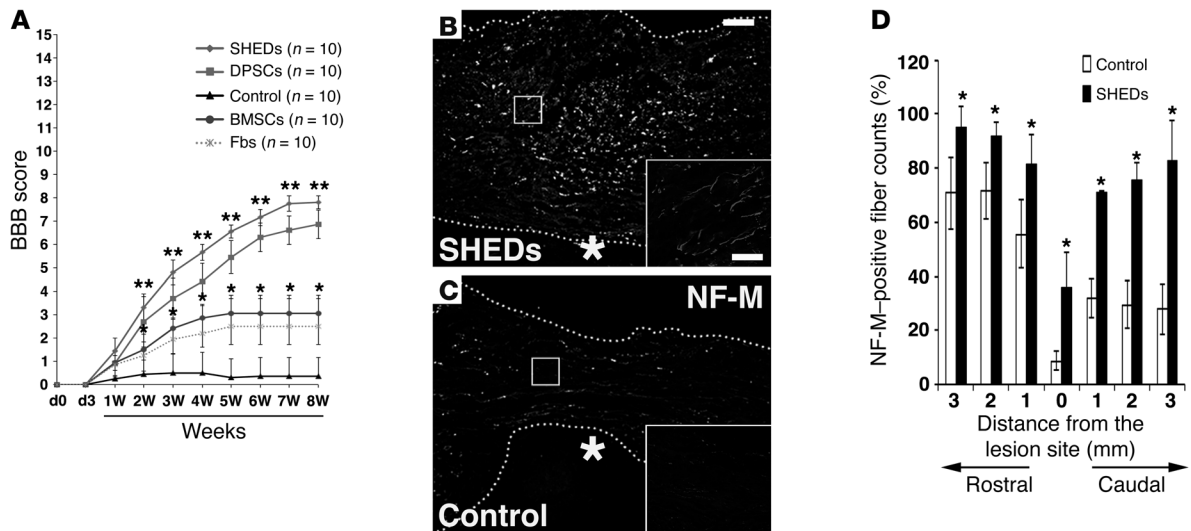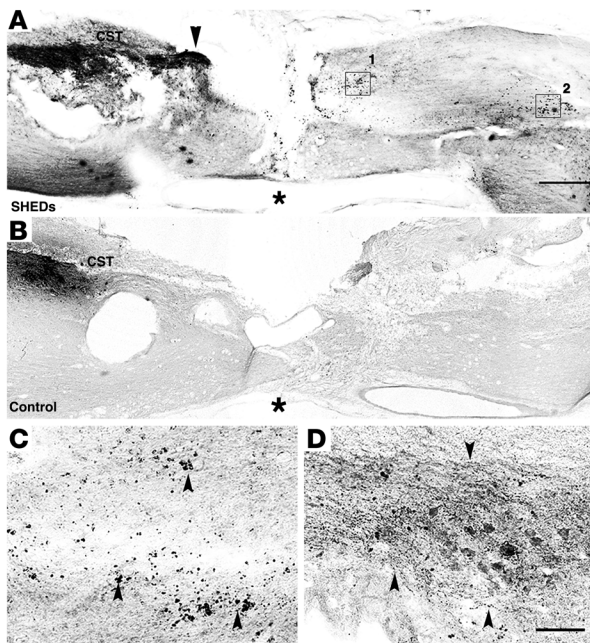
Figure 2
Engrafted SHEDs promote functional recovery of the completely transected SC. (**A**) Time course of functional recovery of hind limbs after complete transection of the SC. A total of 1 × 10⁶ SHEDs, DPSCs, BMSCs, or fibroblasts were transplanted into the SCI immediately after transection. Data represent the mean ± SEM. **$P < 0.001$, *$P < 0.01$ compared with SCI models injected with PBS. (**B**–**D**) Representative images (**B** and **C**) and quantification (**D**) of NF-M–positive nerve fibers in sagittal sections of a completely transected SC, at 8 weeks after SCI. Dashed lines outline the SC. Insets are magnified images of boxed areas in **B** and **C**. (**D**) Nerve fiber quantification, representing the average of 3 experiments performed under the same conditions. The *x* axis indicates specific locations along the rostrocaudal axis of the SC (3 mm rostral and caudal to the epicenter), and *y* axis indicates the percentage of NF-M–positive fibers compared with that of the sham-operated SCs at the ninth thoracic spinal vertebrate (Th9) level. Data represent the mean ± SEM. *$P < 0.05$ compared with SCI models injected with PBS. Scale bars: 100 μm and inset 20 μm (**B**) and 50 μm (**C**). Asterisks in **B** and **C** indicate the epicenter of the lesion.

by paracrine mechanisms; and (c) replacement of lost or damaged oligodendrocytes after SCI through specific differentiation into mature oligodendrocytes under the extreme conditions of SCI. To our knowledge, the latter two neuroregenerative activities (b and c) are unique to tooth-derived stem cells and are not exhibited by any other previously described stem cells. Thus, our data demonstrate that tooth-derived stem cells may provide significant therapeutic benefits for treating the acute phase of SCI through both cell-autonomous and paracrine/trophic regenerative activities.

Adult MSCs have been isolated from various tissues, including bone marrow, adipose tissue, skin, umbilical cord, and placenta (27–30). The therapeutic benefits of these stem cells have drawn intense attention in the field of translational medicine. Nevertheless, their biological equivalency/heterogeneity and identity are largely unknown (31). Tooth-derived stem cells exhibited BMSC-like multipotency and cell surface marker expression; however, they expressed a distinct set of multiple early neural linage markers (Table 1 and Figure 1). A cDNA microarray gene expression analysis showed that the SHEDs expressed many genes in the categories of extracellular and cell surface region, cell proliferation, and tissue/embryonic development, at levels at least 2-fold higher than BMSCs (Table 2). These data indicate that tooth-derived stem cells belong to a highly proliferative ectomesenchymal stem cell–like population that actively communicates with neighboring cells. These characteristics raise the question of what the role of these stem cells is in tooth development and maintenance. Although we do not have a clear answer at present, future analyses using model animals such as dogs and pigs may clarify their precise origin and normal functions, as well as identifying the physiological system that maintains the "stemness" of these cells in vivo.

Both axon regeneration and the reformation of appropriate neuronal connections are prerequisites for functional recovery from SCI. However, multiple AGIs block the inherent regenerative activities of injured axons (2–4). It is well known that multiple AGIs constitute a remarkably intricate molecular network in the extracellular space of the injured CNS, in which they activate a common intracellular signaling mediator, Rho GTPase, and its effector, Rho-associated kinase (ROCK) (32–36). The activation of the Rho-ROCK cascade induces growth cone collapse and axonal repulsion (37). The inactivation of Rho by C3 transferase or of ROCK by Y-27632 downregulates AGI signaling and promotes functional recovery after SCI (38–40). Thus, Rho/ROCK signaling is an important target for SCI treatments; however, no reports have yet described an effect of stem cell transplantation on regulating the multiple AGIs/Rho/ROCK signaling cascades. We found that engrafted SHEDs promoted the regeneration of two major types of descending axons (CST and 5-HT) beyond the lesion epicenter and concomitantly inhibited the SCI-induced Rho activation (Figure 4). Furthermore, both SHED-CM and DPSC-CM promoted the neurite extension of CGNs cultured on two different AGIs, CSPG and MAG (Figure 5). Taken together, these results strongly suggest that tooth-derived stem cells promote the regeneration of transected axons through the direct inhibition of multiple AGI signals by paracrine mechanisms. Notably, in contrast to the CMs from tooth-derived stem cells, BMSC-CM showed only a subtle anti-AGI activity in the neurite extension assay, in good agreement with the level of functional recovery observed in BMSC-transplanted rats. Thus, the anti-AGI activity of tooth-derived stem cells is one of their major therapeutic benefits for the treatment of SCI.

derived stem cells regulate multiple AGI activities to promote the regeneration of injured axons.

It has been shown that pharmacological blockade of neuron and/or oligodendrocyte apoptosis by erythropoietin (41, 42), inhibitors of purine receptor P2X7 (OxATP and PPADS) (43), a neutralizing Ab against CD95 (FAS) antigen (44), or minocycline (45, 46) promotes functional recovery after SCI. We found that engrafted SHEDs suppressed the apoptosis of both neurons and oligodendrocytes (Figure 8), which resulted in the remarkable preservation of neurofilaments and myelin sheaths in the region surrounding the epicenter (Figures 2 and 6). Notably, in addition to these two cell lineages, SHEDs strongly inhibited the apoptosis of astrocytes recruited to the lesion. In the classical view, reactive, CSPG-generating astrocytes are considered to be an obstacle to axon regeneration; however, recent genetic studies in mice have shown that the conditional ablation of astrocytes after SCI resulted in larger lesions, failure of blood brain barrier repair, expansion of the inflammatory response and tissue disruption, severe demyelination, and profound cell death of neurons and oligodendrocytes (47–51). Thus, the accumulated evidence demonstrates that, in addition to their anti-regenerative activity, astrocytes play an important role in the neuroprotection during the acute phase of SCI. We found that SHEDs suppressed the apoptosis of astrocytes and minimized secondary injury but inhibited AGI activity of CSPG derived from activated astrocytes. Thus, these results demonstrate that SHEDs promote the neuroprotective role but inhibit the anti-neuroregenerative activity of astrocytes to promote functional recovery after SCI.

The mechanisms that underlie the inhibition of multiple AGIs by SHED-CM and DPSC-CM are currently unknown. Although both SHEDs and DPSCs expressed an array of neurotrophic factors (Figure 1), our preliminary analysis showed that these trophic factors alone failed to promote the neurite extension of CGNs cultured on CSPG-coated dishes (K. Sakai and A. Yamamoto, unpublished observations). These results suggest that unknown factors, rather than neurotrophic factors, expressed by SHEDs and/or DPSCs may play major roles in the inhibition of multiple AGI signaling pathways. Since the strong anti-AGI activity was unique to the tooth-derived stem cells, but not to BMSCs, extracellular-related genes being preferentially expressed in SHEDs relative to BMSCs (Table 2) is a possible candidate anti-AGI factor. Future functional analysis of these genes will be required to reveal the molecular mechanisms by which tooth-

Figure 4
SHEDs regenerate 5-HT fibers and inhibit SCI-induced activation of Rho GTPase. (**A–D**) Representative images (**A–C**) and quantification (**D**) of serotonergic raphe axons stained with 5-HT mAb in the sagittal sections of the transected SC. A large number of 5-HT axons penetrated the scar tissue of the rostral stump in the SHED-transplanted SC (**A**), while only a few did in the control transected SC (**B**). (**C**) 5-HT–positive boutons were in contact with neurons of the caudal stump. Arrowhead indicates 5-HT–positive fiber extended beyond the epicenter. Quantification of regenerated 5-HT axons (**D**) was carried out as described in Figure 2D, except the y axis indicates the percentage of 5-HT axons compared with that in the sham-operated SC. Data represent the mean ± SEM. *$P < 0.01$ compared with SCI models injected with PBS. Scale bars: 50 μm (**B** and **C**). (**E**) SCI-induced Rho GTPase activation 7 days after SCI was suppressed by engrafted SHEDs. The level of active Rho in lysate from the samples indicated at the top (sham-operated, control, and SHED-transplanted) was examined by RBD pull-down assay.
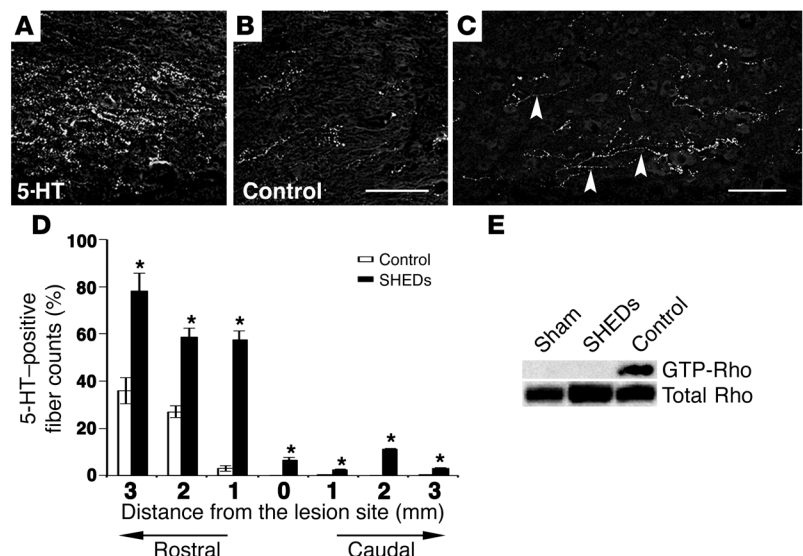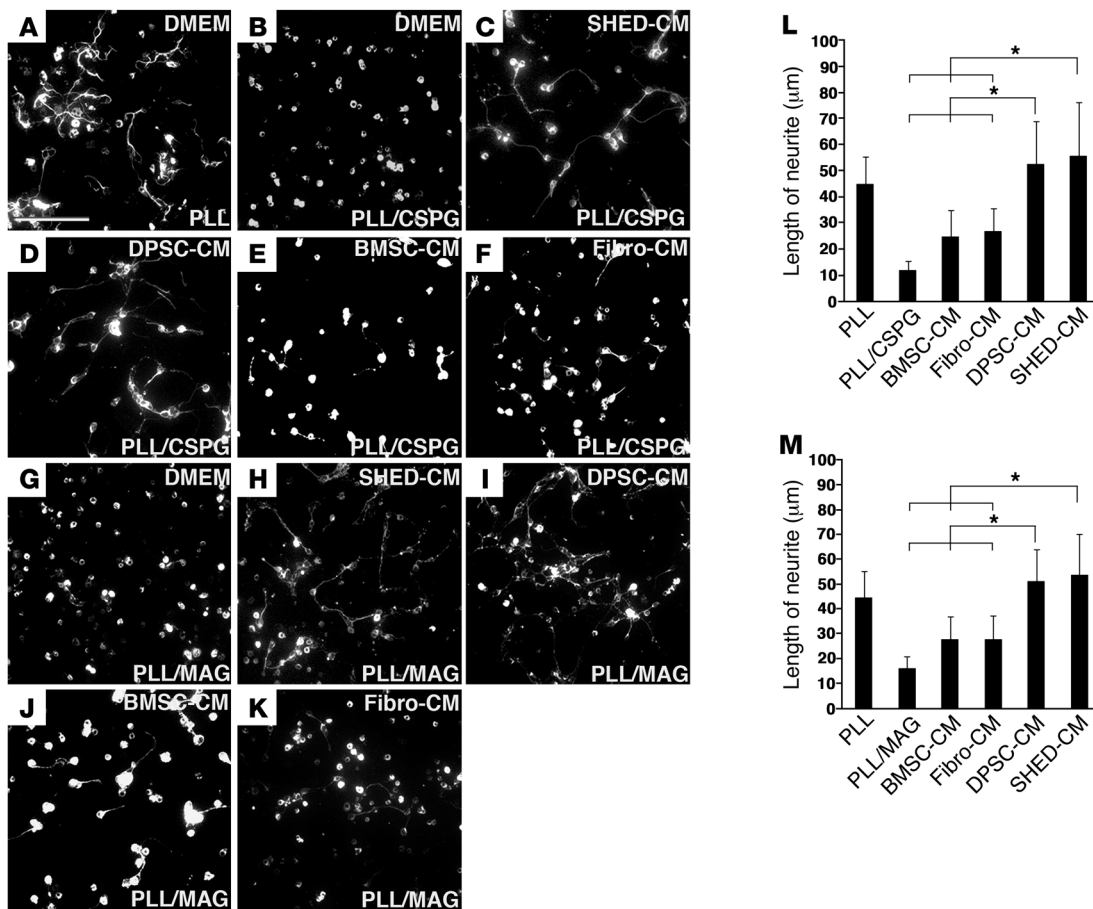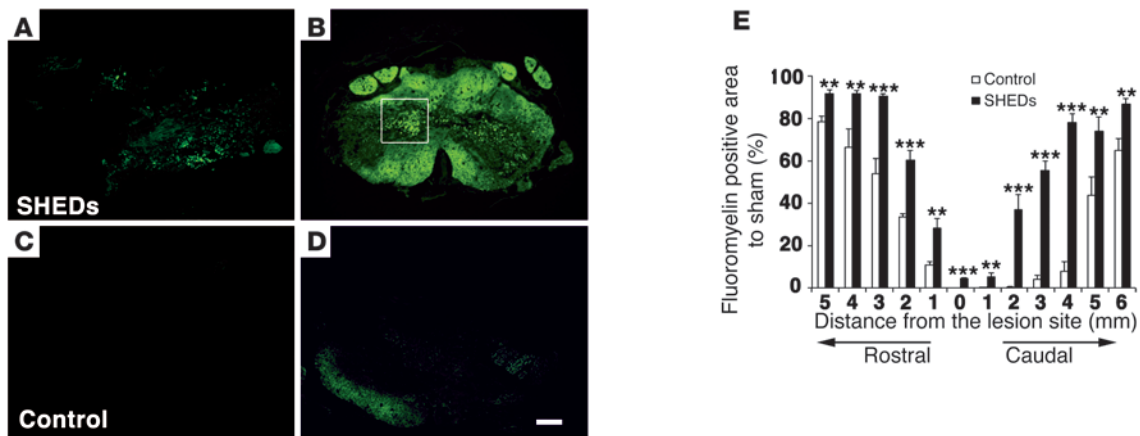
Figure 5
SHED-CM and DPSC-CM promote the neurite extension of CGNs on CSPG or MAG. CGNs were plated on PLL (**A**), PLL /CSPG (**B**–**F**), or PLL /MAG (**G**–**K**), with the CM indicated at the top of each panel. CGNs plated with SHED-CM or DPSC-CM extended their neurites on the CSPG- (**C** and **D**) and MAG-coated (**H** and **I**) dishes, while BMSC-CM and fibroblast-CM (Fibro-CM) elicited only marginal extension on CSPG (**E** and **F**) and MAG (**J** and **K**). Quantification of the neurite length of CGNs plated on CSPG (**L**) and MAG (**M**). The y axis indicates the neurite length. Data represent the average measurements for each cell type from 3 independent donors. This set of experiments was performed 3 times and yielded similar results. Error bars represent SD. *$P < 0.05$. Scale bar in **A** is 100 μm.

Our data revealed two major advantages of using SHEDs for cell replacement in SCI treatment. First, we observed good survival of the engrafted SHEDs: more than 30% of the engrafted SHEDs survived as a cell mass in the injured SC. A previous study reported that, although the experimental details differed from ours, the survival rate of human ES cell–derived oligodendrocytes or motor neurons, transplanted just after complete SC transection, is less than 1% (8). We speculate that the SHED-mediated minimization of secondary injury and/or the formation of cohesive cell clusters of engrafted SHEDs may be attributable to their excellent cell survival rate. Second, we observed that the engrafted SHEDs specifically differentiated toward mature oligodendrocytes, expressing APC and MBP. It has been shown that DPSCs and SHEDs differentiate in vitro toward functionally active neurons that express voltage-gated Na⁺ channels and in vivo toward neuron-like cells 48 hours after their transplantation into the mesencephalon of avian embryos (18). Taken together with our findings, these results support the idea that tooth-derived stem cells exhibit neural stem cell–like characteristics and that unknown environmental cues are important for their fate determination. Since cell-based remy-

elination strategies can restore saltatory conduction and promote functional recovery after SCI (52), the SHED's strong cell survival and oligodendrocyte-specific differentiation potential, particularly under the extreme conditions of SCI, would be great advantages in using these cells to treat SCI. It is hoped that in the future, clarification of the regulatory cues for the specific differentiation of SHEDs will help us to establish efficient therapeutic protocols for SCI patients based on precise cell fate control.

The aim of this study was to address the neuroregenerative activity of tooth-derived stem cells in a particular CNS injury model, SCI. We used the rat complete transection model, because it provides good reproducibility and permits a more accurate assessment of the effects of treatment than do other SCI models. Although contusion and crush models would provide experimental conditions that are closer to the SCIs seen clinically in humans, the amount of injury in these models is not consistent from animal to animal. Furthermore, these incomplete transection models permit spontaneous recovery after SCI, and the residual SC tissues may provide routes for the compensatory sprouting of uninjured SC axons (53). Thus, the transection model was cho-

Figure 6
SHEDs preserve myelin sheath and differentiate into mature oligodendrocytes in the transected SC. Representative images (**A**–**D**) and quantification (**E**) of the myelinated area 8 weeks after SCI. Transverse sections of the epicenter (**A** and **C**) and 3 mm caudal to it (**B** and **D**) were stained with FluoroMyelin. The myelinated area in both regions was significantly preserved in the SHED-transplanted SC (**A** and **B**), but abolished in the control SC (**C** and **D**). Scale bar: 100 μm (**D**). (**E**) Quantification of the myelinated area showing the average of 3 experiments performed in parallel. The x axis indicates specific locations along the rostrocaudal axis of the SC. The y axis indicates the percentage of the myelin-positive area compared with that of the sham-operated SC at the Th9 level. Error bars represent SD. **$P < 0.01$, ***$P < 0.001$ compared with SCI models injected with PBS.

sen as most appropriate for the precise assessment of the axonal regeneration activity of tooth-derived stem cells.

In this study, we transplanted cells into the injured SC immediately after surgical transection, which is impractical for most human SCI cases. We chose this system to examine the therapeutic benefits of the transplanted cells in countering the multiple pathogenic signals that function synergistically during the early phase of SCI. Our future studies will analyze the neuroregenerative activities of tooth-derived stem cells in SCI under more clinically relevant experimental conditions.

In conclusion, we demonstrated multifaceted neuroregenerative activities of tooth-derived stem cells that fulfill many requirements for functional recovery after SCI. Not only did engrafted SHEDs have remarkable neuroregenerative activities, they also showed no malignant transformation 8 weeks after implantation (data not shown). Furthermore, SHEDs and DPSCs can be obtained from exfoliated deciduous and impacted adult wisdom teeth without adverse health effects. Thus, there are few ethical concerns regarding their clinical use. We propose that tooth-derived stem cells may be an excellent and practical cellular resource for the treatment of SCI.

Figure 7
SHEDs differentiate into mature oligodendrocytes in the transected SC. A myelin-positive cell cluster ectopically identified in the medulla of a SHED-transplanted SC (boxed area in Figure 6B) was characterized by immunohistochemical staining with an anti–human nuclei mAb (HuNu) together with Abs against neural cell lineage markers: anti-MBP (**A**–**C**), anti-APC (**D**–**F**), anti-GFAP (**G**–**I**), or anti–NF-M (**J**–**L**). The data indicate that SHEDs specifically differentiate into mature oligodendrocytes. The percentage of the lineage marker–positive to total HuNu-positive cell number (**M**) represents the average of 3 experiments performed in parallel. Error bars represent SD. Scale bar: 100 μm (**L**).
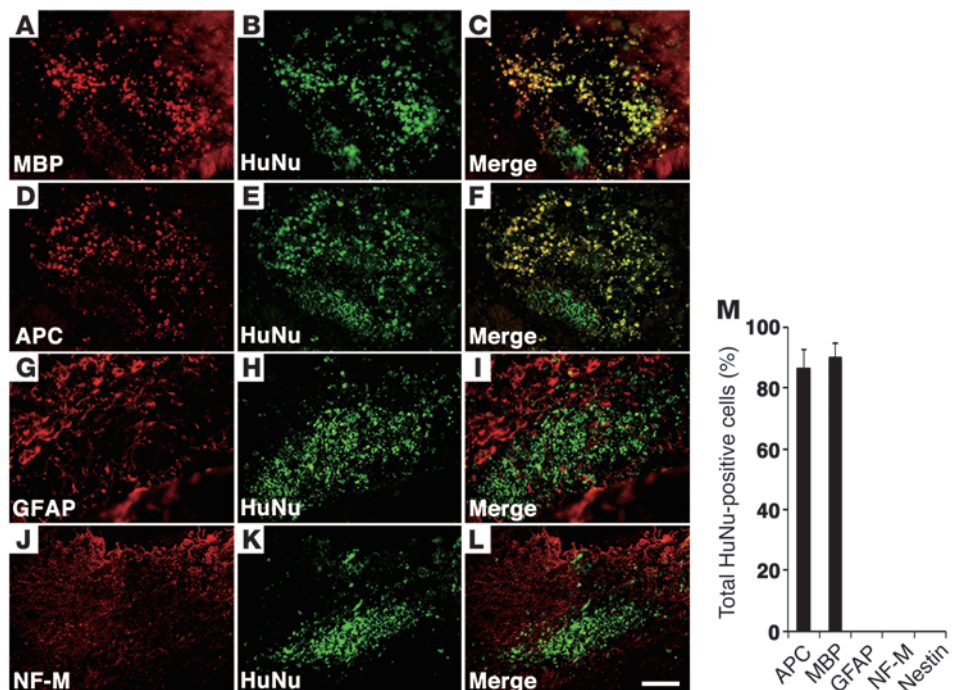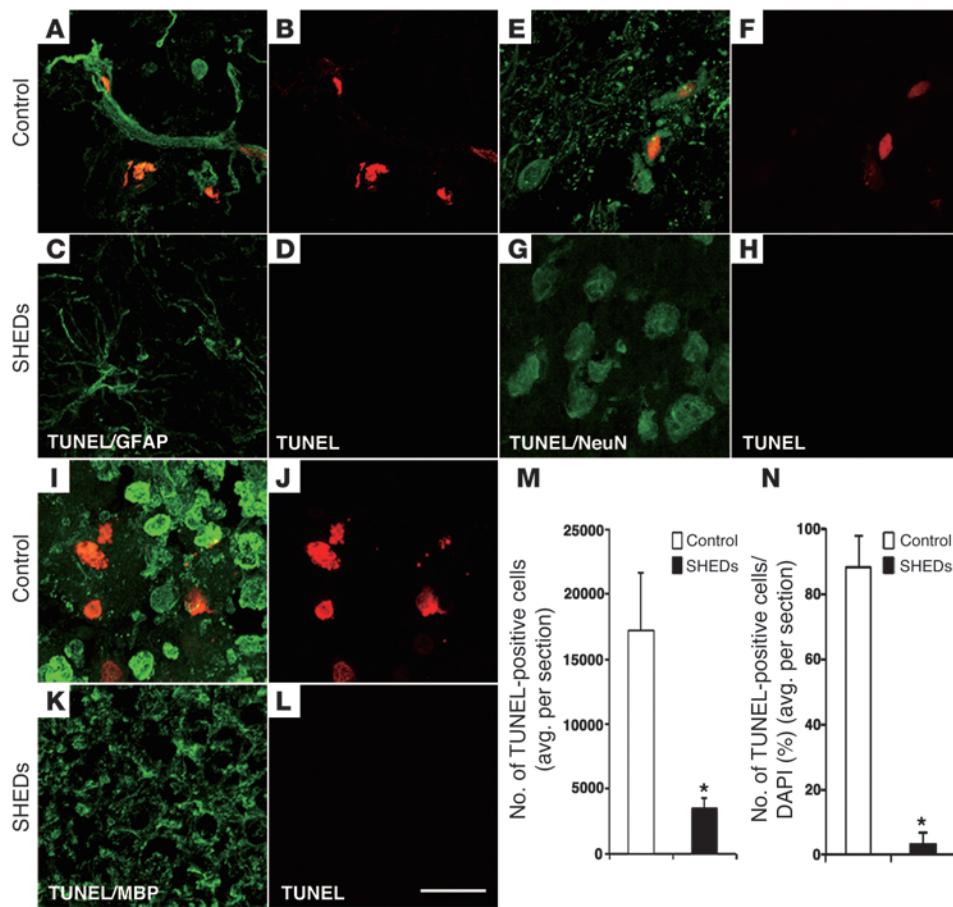
Figure 8
SHEDs suppress the apoptosis of neural cell lineages and secondary injury after SCI. Representative images (**A–L**) and quantifications (**M** and **N**) of apoptotic cell death 24 hours after SCI. Transverse sections 1 mm caudal to the epicenter of PBS-injected (**A**, **B**, **E**, **F**, **I**, and **J**) and SHED-transplanted SCs (**C**, **D**, **G**, **H**, **K**, and **L**) were stained with TUNEL and then subjected to immunohistochemical analysis with an anti-GFAP mAb (**A–D**), anti-NeuN mAb (**E–H**), or anti-MBP mAb (**I–L**). The engrafted SHEDs decreased the apoptotic cell death of all 3 neural cell lineages. (**M**) Quantification of the total TUNEL-positive cell number within 3 mm rostral and caudal to the epicenter shows the average of 3 experiments performed in parallel. (**N**) The percentage of TUNEL-positive relative to total DAPI-positive cell number in the same area as in **M**. Error bars represent SD. *$P < 0.01$ compared with SCI models injected with PBS. Scale bar: 20 μm (**L**).

Methods

Isolation of SHEDs and DPSCs, and cell culture. Human SHEDs and DPSCs were isolated as described previously (16, 17). Briefly, exfoliated deciduous teeth (from individuals 6–12 years old) and adult third molars (18–30 years old) extracted for clinical purposes were collected. After separation of the crown and root, the dental pulp was isolated and then digested in a solution of 3 mg/ml collagenase type I and 4 mg/ml dispase for 1 hour at 37°C. Single-cell suspensions (1×10^4 to 2×10^4 cells/ml) were plated on culture dishes in DMEM supplemented with 10% fetal calf serum, then incubated at 37°C in 5% CO_2. Mesenchymal stem cells of three human bone marrow lines (hBMSCs, from individuals 20–22 years old) at passage 5 and three human skin-fibroblast lines (hFbs, 36–40-years old) at passage 5 were obtained from Lonza and the Health Science Research Resources Bank Japan, respectively.

Real-time PCR and microarray analysis. Total RNA was quantified by a spectrophotometer, and RNA integrity was checked on 1% agarose gels. RT reactions were carried out with Superscript III reverse transcriptase (Invitrogen) using 1 μg of total RNA in a 50 μl total reaction volume. Real-time PCR was performed using the THUNDERBIRD SYBR qPCR Mix (Toyobo) driven by the StepOnePlus Real-Time PCR System (Applied Biosystems). Primers were designed using DNADynamo (BlueTractorSoftware Ltd) and primer 3, as follows: *BDNF* forward (5′-GGGAAAAGGGAACAG-GAAAA-3′), *BDNF* reverse (5′-AACAGACAGGATGGGCAGAA-3′), *GDNF* forward (5′-CGAACTCTTGCCCCTGACCT-3′), *GDNF* reverse (5′-ACAGC-CACGACATCCCATAAC-3′), *CNTF* forward (5′-CCTTCTCTCTTCCTT-GCTTTCTCTT-3′), *CNTF* reverse (5′-TGTCCCTGCTCCCACTCTCT-3′), *NT-3* forward (5′-TCAAAACGGGCAACTCTCCT-3′), *NT-3* reverse (5′-CTC-

GACAAGGCACACACACA-3′), *NGF* forward (5′-TTCCCTTGACACT-GCCCTTC-3′), *NGF* reverse (5′-GATGATGACCGCTTGCTCCT-3′). Microarray experiments were carried out using a CodeLink Human Whole Genome Bioarray (Applied Microarrays Inc.) at Filgen Inc. The arrays were scanned using a GenePix4000B Array Scanner (Molecular Devices). The data were analyzed by using MicroArray Data Analysis Tool version 3.2 (Filgen Inc.) and deposited in the GEO database (accession GSE32403).

Flow cytometry analysis. For flow cytometry, 1×10^6 cells were incubated with FITC-conjugated primary mAbs against CD34, CD45, and CD11b and PE-conjugated against HLA-DR, CD105, CD73, and CD90 (BD Biosciences) at 4°C for 30 minutes and then washed twice with PBS containing 0.1% bovine serum albumin. The expression of intracellular markers was examined by indirect immunostaining. Cells were fixed with 4% (w/v) PFA for 5 minutes and permeabilized with 0.1% (v/v) Triton X-100 in PBS for 5 minutes. After blocking with 10% (v/v) goat serum for 30 minutes, the cells were incubated with primary Abs: anti-GFAP (mouse IgG, 1:500, Millipore), anti–βIII-tubulin (mouse IgG, 1:1,000, R&D Systems), anti-NeuN (mouse IgG, 1:100, Millipore), anti-CNPase (mouse IgG, 1:500, Millipore), anti-nestin (rabbit IgG, 1:500, Millipore), anti-DCX (guinea pig IgG, 1:500, Millipore), anti-APC (rabbit IgG, 1:300, Abcam), anti-MBP (rabbit IgG, 1:500, Abcam), anti-A2B5 mAb (mouse IgG, 1:500, Millipore). The secondary Abs were anti-mouse IgG, anti-rabbit IgG, and anti–guinea pig IgG-conjugated with Alexa Fluor 448 (Invitrogen), used at 1:1,000. Cell fluorescence was evaluated by flow cytometry using a FACSCalibur (BD Biosciences).

Animal model and surgical procedure. Adult female Sprague-Dawley rats were anesthetized with a mixture of xylazine (100–150 mg/kg) and ketamine (60–90 mg/kg). After laminectomy at the 9th–11th thoracic vertebral lev-

els, the dura was opened, and the SC was completely transected using a surgical blade (Feather surgical blade stainless steel no. 11). The severed ends of the SCs typically retracted about 1–2 mm. The rostral and caudal stumps were lifted to ensure complete transection. Then, 1×10^6 cells were drawn into a glass pipette with a tip diameter of 50–70 mm mounted onto a 10-µl Hamilton syringe attached to a micromanipulator. First, the cells were deposited into two injection sites at the rostral and the caudal stumps, 2 mm from the lesion and 0.5 mm lateral to the midline, at a depth of 1.5 mm. A 2.5-µl sample containing 2.5×10^5 cells in PBS was grafted into each site (injection rate, 0.8 µl/min). Next, 1×10^5 cells in fibrin glue were implanted into the 1- to 2-mm gap to fill the lesion site in the severed SC. After surgery, the rats were placed in temperature- and humidity-controlled incubation chambers until they awoke. They were then transferred to cages, and bladder evacuation was applied daily. Antibiotics (sodium ampicillin, 10 mg/kg body weight) were injected into the rats daily for a week. The rats were maintained under postoperative care for 8 weeks. All rats were given cyclosporine (Novartis) at 10 mg/kg/d on the day before surgery transplantation, then every day after surgery.

Immunohistochemical analysis. Cells were plated on PLL-coated 8-chamber slides and then incubated with the primary Abs listed above. For histological examination of the treated SCs, the animals were anesthetized and transcardially perfused with 4% PFA in 0.1 M PBS, 8 weeks after transplantation. The SCs were embedded in OCT compound (Sakura Finetek) and sectioned in the sagittal or transverse plane at 20 µm on a cryostat (Leica). The sections were incubated with primary Abs against human nuclei (mouse IgG, 1:100), NF-M (rabbit IgG, 1:300, Millipore), and 5-HT (rabbit IgG, 1:500, Sigma-Aldrich) in addition to the Abs listed above. Secondary Abs were anti-mouse IgG–Alexa Fluor 488, anti-rabbit IgG–Alexa 546, and anti–guinea pig IgG–Alexa 647. Myelin was stained by FluoroMyelin green dye (Invitrogen), according to the manufacturer's instructions. After counterstaining with DAPI (Sigma-Aldrich), cell images were captured with a confocal laser scanning microscope (A1Rsi, Nikon), while tissue images were taken with a universal fluorescence microscope (BZ9000, Keyence).

The differentiation activity of the engrafted SHEDs and the cells staining positive for MBP, APC, NF-M, or GFAP among the anti–human nuclei–positive transplanted cells were quantified. Cells were counted in at least 15 confocal images from 3 individuals in parallel experiments, with error bars representing SD.

Anterograde neuronal tracing study. For tracing of the CSTs, 0.5 µl of 5% biotinylated dextran amine (BDA: MW 10,000, Molecular Probes, Invitrogen; 5% in PBS) was injected into 4 sites in the hind limb area of the sensorimotor cortex at a 1.2-mm depth, following the rat brain atlas (54). Two weeks after the injections, sagittal cryosections (20 µm thick) of the SCs were prepared and processed by diaminobenzidine (DAB) staining with the ABC reaction protocol (VECTASTAIN Elite ABC, Vector Laboratories).

BBB open field locomotor score. Hind limb neurobehavioral testing was performed using the BBB locomotor rating scale (24). The 22-point (from 0 to 21) BBB scale was used to assess hind limb locomotor recovery, including joint movements, stepping ability, coordination, and trunk stability. A score of 21 indicates unimpaired locomotion as observed in uninjured rats. Two examiners who were blinded to the animal's treatments performed the tests. The duration of each session was 4 minutes per rat. The scores were analyzed by repeated-measures ANOVA with Tukey's multiple comparison tests at each time point.

CM. At 70%–80% confluence, the cell culture medium was changed to serum-free DMEM. After 48 hours incubation at 37°C in 5% CO_2, the CM was collected and centrifuged for 4–5 minutes at 4°C, 22,140 g. After the brief re-centrifugation, the supernatant was collected and used as CM.

Neurite outgrowth assays. Forty-eight-well tissue culture plates (Falcon, BD) were coated with 20 µg/ml PLL (Sigma-Aldrich) and then with 300 ng/ml extracellular CSPG mixture (Millipore) or 400 ng/ml MAG/Fc Chimera (MAG; Sigma-Aldrich) for 4 hours at 37°C. Rat CGNs were seeded onto PLL-, PLL/CSPG-, or PLL/MAG-coated 48-well tissue culture plates at 2.0×10^4 cells/well and cultured at 37°C in 5% CO_2 with SHED-CM, DPSC-CM, BMSC-CM, or fibroblast-CM. After 24 hours incubation, cells were fixed in 4% paraformaldehyde/PBS and stained with anti-neuron-specific βIII-tubulin (R&D Systems) to visualize neurites. Cell processes were defined as neurites when they were longer than the diameter of the cell body. Neurite length was evaluated by manually tracing neurite per cell using ImageJ software (version 1.29, http://rsbweb.nih.gov/ij/) and referenced to a known length. Each experiment was conducted in triplicate, and images were taken with 20 or more cells per field. For each experiment, at least 100 cells were randomly counted and measured.

Analysis of apoptosis. Apoptotic cell death was analyzed by TUNEL assay (In Situ Cell Death Detection kit, Roche). TUNEL-positive cells were counted on sections from sham-treated, PBS-injected, and SHED-transplanted animals. A researcher blinded to the experimental protocol determined the number of TUNEL-positive cells in the entire serial parasagittal section. The average number of TUNEL-positive cells per section was calculated from the values obtained by counting serial sagittal sections through the lesion site of each animal, with 3 animals examined per group.

Statistics. An unpaired 2-tailed Student's *t* test was used for single comparisons. For analysis of the real-time PCR results and open-field scores, we used repeated-measures ANOVA with Tukey's post hoc test (SPSS 19.0). A *P* value less than 0.05 was considered significant.

Study approval. The animal studies were carried out in accordance with the NIH Guidelines for the Care and Use of Laboratory Animals and approved by the Animal Research Committee of Nagoya University. Extracted teeth were collected at the Nagoya University School of Medicine, under approved guidelines set by Nagoya University (H-73, 2003). Ethical approval was obtained from the ethics committee of Nagoya University (permission number 8-2). All participants provided written informed consent.

Address correspondence to: Akihito Yamamoto, Department of Oral and Maxillofacial Surgery, Nagoya University Graduate School of Medicine, 65 Tsurumai-cho, Showa-ku, Nagoya 466-8550, Japan. Phone: 81.52.744.1978; Fax: 81.52.744.1978; E-mail: akihito@med.nagoya-u.ac.jp.

1. Norenberg MD, Smith J, Marcillo A. The pathology of human spinal cord injury: defining the problems. *J Neurotrauma*. 2004;21(4):429–440.
2. Schwab JM, et al. Experimental strategies to promote spinal cord regeneration — an integrative perspective. *Prog Neurobiol*. 2006;78(2):91–116.
3. Rowland JW, Hawryluk GW, Kwon B, Fehlings MG. Current status of acute spinal cord injury pathophysiology and emerging therapies: promise on the horizon. *Neurosurg Focus*. 2008;25(5):E2.
4. Yiu G, He Z. Glial inhibition of CNS axon regeneration. *Nat Rev Neurosci*. 2006;7(8):617–627.
5. Cummings BJ, et al. Human neural stem cells differentiate and promote locomotor recovery in spinal cord-injured mice. *Proc Natl Acad Sci U S A*. 2005; 102(39):14069–14074.
6. Keirstead H, et al. Human embryonic stem cell-derived oligodendrocyte progenitor cell transplants remyelinate and restore locomotion after spinal cord injury. *J Neurosci*. 2005;25(19):4694–4705.
7. Kumagai G, et al. Roles of ES cell-derived gliogenic neural stem/progenitor cells in functional recovery after spinal cord injury. *PLoS One*. 2009;4(11):e7706.
8. Erceg S, et al. Transplanted oligodendrocytes and motoneuron progenitors generated from human embryonic stem cells promote locomotor recovery after spinal cord transection. *Stem Cells*. 2010; 28(9):1541–1549.
9. Hofstetter CP, et al. Marrow stromal cells form guiding strands in the injured spinal cord and promote recovery. *Proc Natl Acad Sci U S A*. 2002; 99(4):2199–2204.
10. Cizkova D, Rosocha J, Vanicky I, Jergova S, Cizek M. Transplants of human mesenchymal stem cells improve functional recovery after spinal cord injury in the rat. *Cell Mol Neurobiol*. 2006; 26(7–8):1167–1180.
11. Sharp J, Keirstead HS. Therapeutic applications of oligodendrocyte precursors derived from human embryonic stem cells. *Curr Opin Biotechnol*. 2007; 18(5):434–440.
12. Deshpande DM, et al. Recovery from paralysis in adult rats using embryonic stem cells. *Ann Neurol*. 2006;60(1):32–44.
13. Kopen GC, Prockop DJ, Phinney DG. Marrow stromal cells migrate throughout forebrain and cerebellum, and they differentiate into astrocytes after injection into neonatal mouse brains. *Proc Natl Acad Sci U S A*. 1999;96(19):10711–10716.
14. Furuya T, et al. Treatment of rat spinal cord injury with a Rho-kinase inhibitor and bone marrow stromal cell transplantation. *Brain Res*. 2009; 1295:192–202.
15. Gronthos S, et al. Stem cell properties of human dental pulp stem cells. *J Dent Res*. 2002;81(8):531–535.
16. Gronthos S, Mankani M, Brahim J, Robey PG, Shi S. Postnatal human dental pulp cells (DPSCs) in vitro and in vivo. *Proc Natl Acad Sci U S A*. 2000;97(25):13625–13630.
17. Miura M, et al. SHED: stem cells from human exfoliated deciduous teeth. *Proc Natl Acad Sci U S A*. 2003;100(10):5807–5812.
18. Arthur A, Rychkov G, Shi S, Koblar SA, Gronthos S. Adult human dental pulp stem cells differentiate toward functionally active neurons under appropriate environmental cues. *Stem Cells*. 2008; 26(7):1787–1795.
19. Wang J, et al. Stem cells from human-exfoliated deciduous teeth can differentiate into dopaminergic neuron-like cells. *Stem Cells Dev*. 2010; 19(9):1375–1383.
20. Nosrat IV, Widenfalk J, Olson L, Nosrat CA. Dental pulp cells produce neurotrophic factors, interact with trigeminal neurons in vitro, and rescue motoneurons after spinal cord injury. *Dev Biol*. 2001; 238(1):120–132.
21. Nosrat IV, Smith CA, Mullally P, Olson L, Nosrat CA. Dental pulp cells provide neurotrophic support for dopaminergic neurons and differentiate into neurons in vitro; implications for tissue engineering and repair in the nervous system. *Eur J Neurosci*. 2004;19(9):2388–2398.
22. Huang AH-C, Snyder BR, Cheng P-H, Chan AWS. Putative dental pulp-derived stem/stromal cells promote proliferation and differentiation of endogenous neural cells in the hippocampus of mice. *Stem Cells*. 2008;26(10):2654–2663.
23. Arthur A, Shi S, Zannettino AC, Fujii N, Gronthos S, Koblar SA. Implanted adult human dental pulp stem cells induce endogenous axon guidance. *Stem Cells*. 2009;27(9):2229–2237.
24. Basso DM, Beattie MS, Bresnahan JC. A sensitive and reliable locomotor rating scale for open field testing in rats. *J Neurotrauma*. 1995;12(1):1–21.
25. Mirsky R, Winter J, Abney ER, Pruss RM, Gavrilovic J, Raff MC. Myelin-specific proteins and glycolipids in rat Schwann cells and oligodendrocytes in culture. *J Cell Biol*. 1980;84(3):483–494.
26. Bhat RV, et al. Expression of the APC tumor suppressor protein in oligodendroglia. *Glia*. 1996; 17(2):169–174.
27. In 't Anker PS, et al. Isolation of mesenchymal stem cells of fetal or maternal origin from human placenta. *Stem Cells*. 2004;22(7):1338–1345.
28. Romanov YA, Svintsitskaya VA, Smirnov VN. Searching for alternative sources of postnatal human mesenchymal stem cells: candidate MSC-like cells from umbilical cord. *Stem Cells*. 2003; 21(1):105–110.
29. Young HE, et al. Human reserve pluripotent mesenchymal stem cells are present in the connective tissues of skeletal muscle and dermis derived from fetal, adult, and geriatric donors. *Anat Rec*. 2001; 264(1):51–62.
30. Zuk PA, et al. Human adipose tissue is a source of multipotent stem cells. *Mol Biol Cell*. 2002; 13(12):4279–4295.
31. Nombela-Arrieta C, Ritz J, Silberstein LE. The elusive nature and function of mesenchymal stem cells. *Nat Rev Mol Cell Biol*. 2011;12(2):126–131.
32. Maekawa M, et al. Signaling from Rho to the actin cytoskeleton through protein kinases ROCK and LIM-kinase. *Science*. 1999;285(5429):895–898.
33. Winton MJ, Dubreuil CI, Lasko D, Leclerc N, McKerracher L. Characterization of new cell permeable C3-like proteins that inactivate Rho and stimulate neurite outgrowth on inhibitory substrates. *J Biol Chem*. 2002;277(36):32820–32829.
34. Yamashita T, Tohyama M. The p75 receptor acts as a displacement factor that releases Rho from Rho-GDI. *Nat Neurosci*. 2003;6(5):461–467.
35. Monnier PP, Sierra A, Schwab JM, Henke-Fahle S, Mueller BK. The Rho/ROCK pathway mediates neurite growth-inhibitory activity associated with the chondroitin sulfate proteoglycans of the CNS glial scar. *Mol Cell Neurosci*. 2003;22(3):319–330.
36. Dubreuil C, Winton M, McKerracher L. Rho activation patterns after spinal cord injury and the role of activated Rho in apoptosis in the central nervous system. *J Cell Biol*. 2003;162(2):233–243.
37. Hall A. Rho GTPases and the actin cytoskeleton. *Science*. 1998;279(5350):509–514.
38. Lehmann M, et al. Inactivation of Rho signaling pathway promotes CNS axon regeneration. *J Neurosci*. 1999;19(17):7537–7547.
39. Dergham P, Ellezam B, Essagian C, Avedissian H, Lubell WD, McKerracher L. Rho signaling pathway targeted to promote spinal cord repair. *J Neurosci*. 2002; 22(15):6570–6577.
40. Fournier AE, Takizawa BT, Strittmatter SM. Rho kinase inhibition enhances axonal regeneration in the injured CNS. *J Neurosci*. 2003;23(4):1416–1423.
41. Celik M, et al. Erythropoietin prevents motor neuron apoptosis and neurologic disability in experimental spinal cord ischemic injury. *Proc Natl Acad Sci U S A*. 2002;99(4):2258–2263.
42. Gorio A, et al. Recombinant human erythropoietin counteracts secondary injury and markedly enhances neurological recovery from experimental spinal cord trauma. *Proc Natl Acad Sci U S A*. 2002; 99(14):9450–9455.
43. Wang X, et al. P2X7 receptor inhibition improves recovery after spinal cord injury. *Nature Med*. 2004; 10(8):821–827.
44. Demjen D, et al. Neutralization of CD95 ligand promotes regeneration and functional recovery after spinal cord injury. *Nature Med*. 2004;10(4):389–395.
45. Stirling DP, et al. Minocycline treatment reduces delayed oligodendrocyte death, attenuates axonal dieback, and improves functional outcome after spinal cord injury. *J Neurosci*. 2004;24(9):2182–2190.
46. Teng YD, et al. Minocycline inhibits contusion-triggered mitochondrial cytochrome c release and mitigates functional deficits after spinal cord injury. *Proc Natl Acad Sci U S A*. 2004;101(9):3071–3076.
47. Bush TG, et al. Leukocyte infiltration, neuronal degeneration, and neurite outgrowth after ablation of scar-forming, reactive astrocytes in adult transgenic mice. *Neuron*. 1999;23(2):297–308.
48. Faulkner JR, Herrmann JE, Woo MJ, Tansey KE, Doan NB, Sofroniew MV. Reactive astrocytes protect tissue and preserve function after spinal cord injury. *J Neurosci*. 2004;24(9):2143–2155.
49. Okada S, et al. Conditional ablation of Stat3 or Socs3 discloses a dual role for reactive astrocytes after spinal cord injury. *Nature Med*. 2006; 12(7):829–834.
50. Herrmann JE, et al. STAT3 is a critical regulator of astrogliosis and scar formation after spinal cord injury. *J Neurosci*. 2008;28(28):7231–7243.
51. Rolls A, Shechter R, Schwartz M. The bright side of the glial scar in CNS repair. *Nat Rev Neurosci*. 2009;10(3):235–241.
52. Keirstead HS. Stem cells for the treatment of myelin loss. *Trends Neurosci*. 2005;28(12):677–683.
53. Thuret S, Moon LDF, Gage FH. Therapeutic interventions after spinal cord injury. *Nat Rev Neurosci*. 2006;7(8):628–643.
54. Paxinos G, Watson C. *The Rat Brain in Stereotaxic Coordinates*. 2nd ed. Orlando, Florida, USA: Academic Press; 1986.